ACS APPLIED MATERIALS & INTERFACES

RESEARCH ARTICLE

www.acsami.org

Amontonian Friction Induced by Flexible Surface Features on Microstructured Silicon

Esben Thormann,*[,†] Sang Ho Yun,[‡] Per M. Claesson,[†,§] and Jan Linnros[‡]

[†]Department of Chemistry, Surface and Corrosion Science, Royal Institute of Technology, Drottning Kristinas Väg 51, SE-100 44 Stockholm, Sweden

[‡]Materials Physics, ICT School, Royal Institute of Technology Electrum 229, SE-164 40 Kista, Sweden

[§]Institute for Surface Chemistry, YKI, P.O. Box 5607, SE-114 86 Stockholm, Sweden

ABSTRACT: Friction between nonadhering sliding surfaces are normally described by Amontons' law, which states that there exists a linear relationship between the friction force and the normal applied load and that the friction force is independent of the macroscopic contact area between the surfaces and the sliding velocity. In this study we have measured friction as a function of applied load between a spherical silica particle and a microstructured silicon surface consisting of arrays of vertical microneedles, and we have challenged Amontons' law by changing the size of the silica particle and the sliding velocity. First, when looking at the friction as a function of time for a given applied load, the friction force was observed to oscillate with a period related to the spacing between the microneedles when using a small silica particle, whereas the friction force exhibited a more random variation when a larger silica particle was used. The oscillation in the friction force is a direct evidence for bending and release of individual microneedles and the observation illustrates that the energy dissipating mechanism becomes hidden in the friction data when the dimensions of the sliding body becomes much larger than the length scale of the surface features causing the friction. Second, when looking at the average friction force as a function of applied load we find, in accordance with Amontons' law, a linear relationship between the friction force and the applied load and the friction force is independent of both the size of the sliding silica particle and of the sliding velocity. One exception from this, however, was observed when sliding a small silica particle at low velocity, where a deviation from Amontons' law was noticed. The deviation from Amontons' law is suggested to be attributed to a change in the energy dissipating mechanism giving rise to the friction force. In light of that it is suggested that Amontons' law only is valid as long as the main energy dissipating mechanism does not change with the applied load. To get a better understanding of the general validity of Amontons' law, our results were evaluated against different microscopic models.

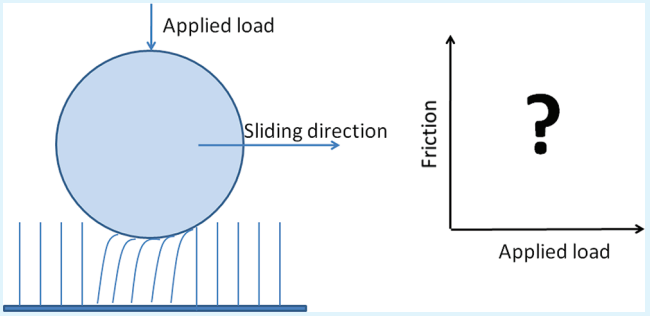

KEYWORDS: friction, Amontons' law, sliding velocity, contact area, surface structure, elastic deformation

1. INTRODUCTION

The concept of friction has through modern human history challenged engineers and fascinated scientists. The first documented systematic friction studies are dated back to the 15th century, where Leonardo da Vinci performed experiments that demonstrated that the friction force apparently is proportional to the applied load and independent of the macroscopic contact area between the sliding bodies. Two hundred years later, these findings were rediscovered by Guillaume Amontons and even later verified by Charles-Augustin de Coulomb, and merged to the today well-known law of friction, Amontons' law. This law states that the friction force is given as

$$F_{\mathrm{fric}} = \mu F_{\mathrm{N}} \qquad (1)$$

where F_{fric} and F_{N} are the friction force and normal applied load, respectively, and μ is known as the friction coefficient, which is a constant related to the nature of the sliding bodies but independent of their macroscopic contact area and the sliding velocity.

Despite its simplicity and lack of theoretical foundation, Amontons' law has been very successfully applied to a large range of different types of materials.[1] Also, friction between both atomically mooth surfaces[2−5] and surfaces with different degrees of roughness[6−9] friction measured at different humidities,[10−13] in different solvents[14−16] or in the presence of lubricating agents;[17−20] and recently, friction measured between a range of nanostructured surfaces[21] has all shown to be in accordance with Amontons' law. Only in the case of strongly adhesive contact between the sliding surfaces, and when covering a very large range of applied loads, does Amontons' law seems to fail.[4,11,22,23]

There have been a large number of attempts to give a microscopic explanation to Amontons' law and especially the largest intellectual challenge, namely the apparent independence between friction and the interacting area of the sliding bodies.

Received: May 23, 2011
Accepted: August 10, 2011
Published: August 10, 2011

In 1950, Bowden and Tabor[22] suggested that friction is indeed related to the real contact area and that the validity of Amontons' law is a consequence of surface roughness which causes the real contact area to increase with the applied load. This was shown to give a result in accordance with Amontons' law if plastic deformation between all surface junctions was assumed. A similar approach was taken by Greenwood and Williamson,[24] who reached the result that the real contact area scales linearly with the applied load when assuming elastic deformable surface asperities with a Gaussian height distribution. Recently, extended molecular dynamics simulations have demonstrated that Amontons' law is fulfilled for nonadhering atomically smooth surfaces because of a linear relationship between applied load and the number of atomic contact points.[25,26] However, the linear coupling between applied load and true contact area seems in all cases to be model and system dependent, and thus not in good agreement with the experientially observed robustness of Amontons' law.

Today, new types of topographically structured surfaces are being developed for various applications.[31−34] Because such surfaces normally are very susceptible to wear processes the issue of understanding the connection between friction and load is as relevant as ever. In the present study, we will challenge Amontons' law with a surface with topographical microstructure where the number of macroscopic contact point does not vary with the applied load but is proportional to the size of the sliding body. This is done by measuring friction between a silica particle and a microstructured silicon surface consisting of arrays of vertical needles with a height and spacing of approximate 3 and 1.4 μm, respectively (see Figure 1). By varying the applied load, the size of the silica particle (d = 7 an 28 μm) and the sliding velocity between the particle and the microstructured surface we are able to test all three aspects of Amontons' law, namely, the linearity between friction force and applied load, and the independence of the apparent contact area and sliding velocity. The sample and probe dimensions were chosen so that the smaller probe only will be in contact with at small number of asperities at any given time, whereas the larger probe will be in contact with many asperities. The length scale of the spacing between the individual microneedles further makes it possible to resolve the interaction with individual needles, whereas the choice of a sample design with thin flexible surface features compared to more robust structures enable an investigation of how a microscopic elastic deformation contributes to the overall friction force.

2. MATERIALS AND METHODS

Surface Preparation. A microstructured silicon surface consisting of arrays of vertical silicon microneedles was fabricated by reactive ion etching with the Bosch process which is commonly applied for the fabrication of deep pore and trench arrays.[27] A 1 μm-thick oxide layer as an etching mask was capped on a Si (100) wafer. The patterning of SiO_2/Si was generated by photolithography followed by reactive ion etching. SF_6 and C_4F_8 in the etching process were used as etching and passivating gas, respectively. A scanning electron microscope (SEM) analysis has revealed that the needles have an approximate hight of 3 μm and are sitting in a square lattice with a nearest neighbor distance of approximately 1.4 μm. Figure 1 show tilted SEM images of the microstructured surface. Before use the surface was cleaned in water and ethanol and plasma cleaned for 30 s using a Harrick PDC-32G-2 plasma cleaner (Harrick Plasma, USA) at medium intensity (700 V, 15 mA DC). Additionally it should be noted that the microstructured silicon surface did not have any grown oxide layer and is thus naturally hydrophobic. However, a thin native oxide layer normally quickly appears on a silicon surface and after the cleaning procedure this surface exhibited a water contact angle of approximately 70°. This indicates a relatively low surface energy, which is thus expected to limit possible capillary effects.

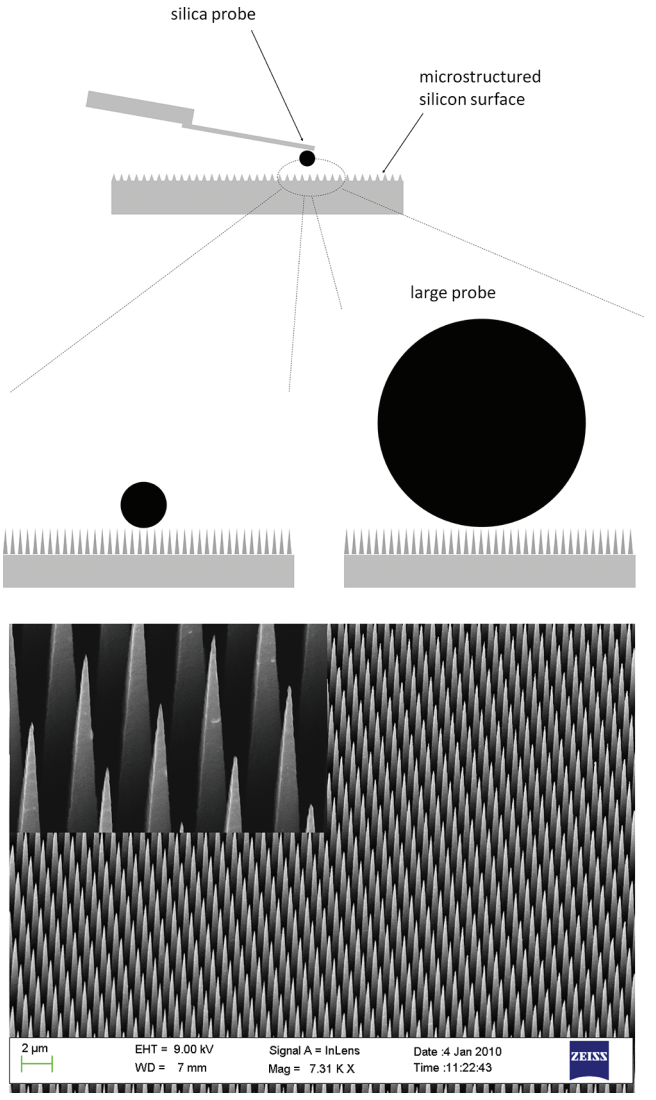

Figure 1. Top: Schematic illustration of our experimental setup. Friction is measured between a silica particle glued to an AFM cantilever and a microstructured silicon surface consisting of arrays of vertical silicon microneedles. In the experiments, we have used two different sizes of the silica particle, where the smallest (d = 7 μm) has a size that is only slightly larger the spacing between the needles and the largest (d = 28 μm) covers many needles at any given moment. Bottom: Scanning electron microscope images of the microstructured silicon surface consisting of a microneedles with an approximate height of 3 and a spacing of 1.4 μm.

Friction Measurements. Measurements of the friction force versus applied load were carried out in air (T=21 °C, RH≈30%) using an atomic force microscope (Nanoscope Multimode III equipped with a Pico Force controller and a scanner with closed loop in the normal direction, Veeco Instruments Inc.). Colloidal probe cantilevers were made by attaching a silica particle to a tipless rectangular cantilever (NSC 12, F-lever, MikroMasch) with a high-temperature melting epoxy glue (Shell Epikote 1009) by use of an Ependorf Micromanipulator 5171 and a Nikon Optiphot 100S reflection microscope. This microscope was also used to measure the size of the attached silica particles. For this study two cantilevers with 7 and 28 μm attached silica particles was

prepared. Smaller probes are not preferable if one wants to ensure that we solely are going to have contact between the probe and the microneedles and not between the microneedles and the cantilever itself. Before particle attachment, the normal and torsional spring constants of the cantilevers were determined by the Sader method as described elsewhere.[28] The cantilever dimension and stiffness were chosen such that the maximum applied normal load was not leading to a cantilever deflection outside the linear region of the detector.[29] Further, as will be discussed in more detail later, a cantilever with a large torsional spring constant is essential in situations where mechanical instability of the lateral movement of the cantilever occurs.

Friction force measurements were performed by obtaining a series of contact mode images each containing 16 trace and retrace lines and saving torsional cantilever deflection data. From the knowledge of the probe size, the torsional sensitivity and spring constant and the normal sensitivity and spring constant, the torsional cantilever deflection was converted to friction force and the normal deflection to applied load. During the scans we kept a relatively low feedback gain ensuring a given average applied load but allowing smaller local variations in load. During the scans, we keedback gain, ensuring a given average applied load but allowing smaller local variations in load. It was further observed that the torsional deflection signal was insensitive to the gain settings as long as the gain was not so low that the probe loses surface contact or so high that the piezo overcompensates for height changes. To obtain the friction force as a function of normal load, we systematically changed the deflection set point in between each image. Further, to obtain the average friction force versus normal load, we averaged the data from the 16 traces and retraces (each containing 512 points) to provide a single value for each value of applied load. In each case, the friction versus normal load measurements were repeated three times to verify the data and to exclude wear. These repeated measurements are also used to calculate the uncertainty in the determined friction coefficients. It should be noted that in this study, we define the friction force as the lateral force measured while moving the probe parallel to the sample substrate under an average applied force. This definition is in agreement with the macroscopic friction force resisting the movement of a body parallel to a rough surface under a given applied load but is not identical to the local microscopic friction response which is parallel to the tangent of a given surface feature but not to the sample substrate.

The lateral photodetector sensitivity was calibrated using the method of tilting the AFM head as suggested by Pettersson et al.[30] The scan length for the friction measurement were set to 40 μm to ensure that a reasonable number of microneedles were passed in each scan line. The scanning velocity was varied in four steps; 8, 80, 400, and 800 μm/s. The friction measurements were in all cases performed parallel to the orientation of the arrays of microneedles in the square lattice to ensure the same distance between the needles as seen from the scanning direction. This alignment was done by aligning lines on the surface, originating from the etching mask, with the cantilever under an optical microscope built into the AFM setup.

Results and Discussion. *Local Friction Response.* Panels A, C, and E Figure 2 show examples of friction data obtained, at an applied load of approximately 120 nN, in air between silica probes of different sizes and a flat silica surface and the microstructured surface, respectively. These plots illustrate single friction traces and retraces obtained over a 40 μm scan in 1 s (0.5 s for each trace and retrace, respectively), together with the averaged traces and retraces sampled under 16 subsequent scans. Each trace and retrace were from the time domain analyzed by performing a discrete Fourier transformation

$$F_n = \sum_{k=0}^{N-1} f_k e^{-2\pi i n k/N} \quad (2)$$

where N is the number of sampling points in a scan line and f_k is the inverse transform. From this expression, the complex modulus, also commonly known as the power spectrum, is defined as

$$\text{power} = (F_n \cdot \bar{F}_n)^{-1/2} \quad (3)$$

where $\bar{F}_n$ is the complex conjugate of the discrete Fourier transform. These power spectra are shown for each of the 16 scan lines in panels B, D, and F in Figure 2.

In the case of shearing a d = 28 μm silica probe against a flat silicon surface (Figure 2A), an almost constant friction force is observed and the Fourier analysis (Figure 2B) reveals only low-intensity and low-frequency random noise. Although part of the total friction force is expected to be a result of surface irregularities or surface roughness, these experiments show that such features cannot be directly resolved on the time and length scale of this experiment.

In the case of shearing a d = 7 μm silica probe against the microstructured surface (Figure 2C), the friction force is no longer constant but shows an apparent oscillatory behavior with a number of periods which equals the expected number of microneedles being past during a 40 μm scan. We interpret this observation as follows; shearing the probe against the surface leads to bending of the needles and each oscillatory period corresponds to bending and releasing individual needles. This also suggests that only a few needles at the time provides a significant contribution to the total friction force and because of this discreteness in the interaction, we can in this experiment resolve the structure of the surface from the friction data. The Fourier analysis (Figure 2D) presents a clear peak, repeated in all 16 scan lines, with a maximum of 62 Hz, which with a 40 μm scan in 0.5 s corresponds to a distance of 1.3 μm. This distance correlates well with the approximate distance of 1.4 μm between two neighboring needles determined from the SEM images. Here it should be noted that the small difference between the distance from the SEM analysis and the oscillatory period in the friction force is of the same order of magnitude as the lateral resolution in our friction measurements.

In the case of shearing a d = 28 μm silica probe against the microstructured surface (Figure 2E) the friction force has a higher noise level than in the case of a flat silica surface but does not show the same oscillatory behavior as in the case of using the d = 7 μm silica probe. The high noise level is also revealed by the Fourier analysis (Figure 2F). In this case peaks at different frequencies are found in different scan lines, but no systematically repeating peak around 62 Hz or at other frequencies are observed. Thus, by going from a 7 μm probe to a 28 μm probe, we lose the ability to resolve the individual bending event. This means that even if we know that the friction force is a result of the same energy dissipating mechanism in the two cases, we do not see any direct evidence of this when using the larger probe. This corresponds to shearing surfaces with small-scaled random roughness, where the friction force is dependent on the surface structure, but where the surface features cannot be resolved in the friction data.

It should be noted that in cases where stick and slip motion occurs as in the present case where a needle presumable first is bent and then subsequently released, a mechanical instability of the measuring system will be found. When the needle bends, it will act with a restoring force on the silica particle leading to some cantilever deflection. When the needle is released, the cantilever will thus for a short time interval be in a mechanical unstable situation until the force balance is restored. This leads to small gaps in the data where the equilibrium cantilever deflection is unknown. A parallel to this is known from normal force measurements where mechanical instabilities of the cantilever can lead to so-called "jump-in" and "jump-out" events.[35] In the case of normal force measurements, the jump length can be reduced by choosing a cantilever with a normal spring constant which is large relative to the gradient of the force. In the present case, the jump length can be reduce by choosing a cantilever with a torsional spring constant which is large compared to the bending stiffness of the microneedles. This is the reason for choosing a relatively stiff cantilever in this study as noted in the Materials and

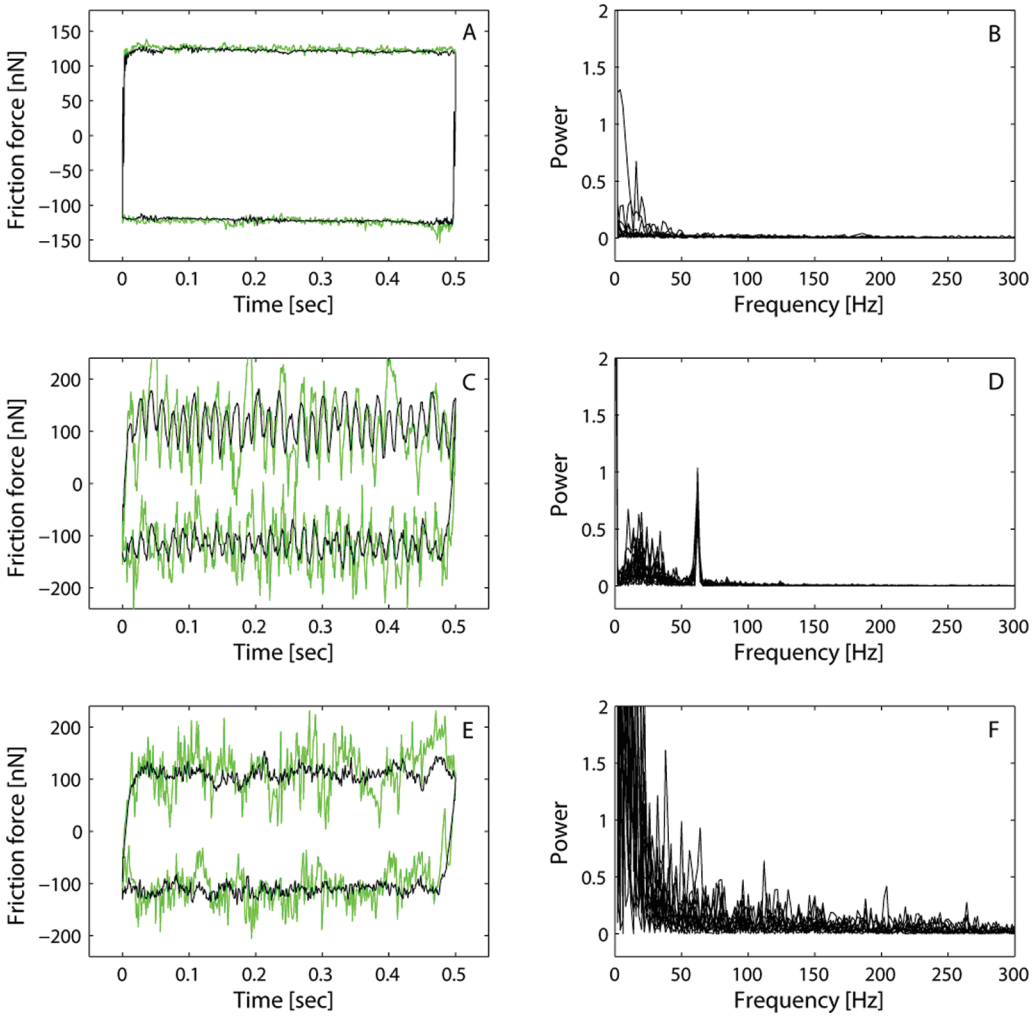

Figure 2. Left panels show the friction force versus time obtained for a scan over 40 μm between (A) a 28 μm silica probe and a flat silicon surface, (C) a 7 μm silica probe and microstructured silicon surface, and a 28 μm silica probe, and (E) microstructured silicon surface. Right panels show the result of a Fourier analysis of friction versus time data for 16 consecutive lines obtained for each of the three situations.

Methods section. An exact determination of the degree of bending is difficult due to the undefined geometry of the needles and the uncertainty of the exact loading point. However, for a silicon rod of the approximate same dimension exposed to an end loaded force of 200 nN, corresponding to the highest local lateral force, the deflection would be around $\Delta x_{\text{needle}} = Fl^3/(3EI) \approx 100$ nm.[37] In comparison the displacement of the probe due to the torsional deflection of the cantilever, $\Delta x_{\text{probe}} = d^2F/k_t \approx 1$ nm, for the $d = 7$ μm probe and 10 nm for the $d = 28$ μm probe.[37]

Average Friction versus Applied Load. In the previous section, we discussed the local friction response in terms of its time dependence and spatial variation. However, Amontons' law is a macroscopic law and thus refers to a time- and space-average of the observations discussed above. The average friction force between the $d = 7$ μm and the $d = 28$ μm silica probe, respectively, and the microstructured surface was determined by performing a time- and space-average at each value of applied load as described in the Materials and Methods section. Panels A and B in Figure 3 display the average friction force versus normal load at four different sliding velocities ranging 8−800 μm/s for the two different probe sizes. The friction force was measured both upon increasing and decreasing applied load, but no significant difference was observed.

In the case of shearing a $d = 7$ μm silica probe against the microstructured surface (Figure 3A), a linear relation between friction and applied load, in accordance with Amontons' law, is found for sliding velocities in the range 80−800 μm/s. Further, for the three largest sliding velocities, the friction force is found to be independent of the sliding velocity and thus we find the same friction coefficient, $\mu = 0.93 \pm 0.04$, in all three cases (compared to $\mu = 0.51 \pm 0.07$ measured between the probe and flat silicon[36]). Further, the fact that the friction force is close to zero at zero applied load indicates that adhesion, e.g., capillary adhesion, does not significantly contribute to the friction. If the average friction force is an effect of bending the microneedles and intrinsic friction between the contact surfaces, then the friction force is expected to be independent of the sliding velocity as long as the feedback is sufficiently high to ensure that the probe is not "flying" over the surface features. Thus, in the present case, it can be concluded that the probe stays in contact with the surface features to the same degree at the three highest sliding velocities. However, for the lowest sliding velocity, $v = 8$ μm/s, the behavior is somewhat different. At low applied loads, the friction force follows the same trend as for higher sliding velocities, whereas at higher applied loads, the average friction force starts to diverge, showing lower values than at higher sliding velocities. The same behavior was observed in three repeated measurements. Such a change in friction has to reflect a change in the interaction between the probe and the microneedles; because the measured friction decreases, an obvious suggestion would be that the needles become less bent in the

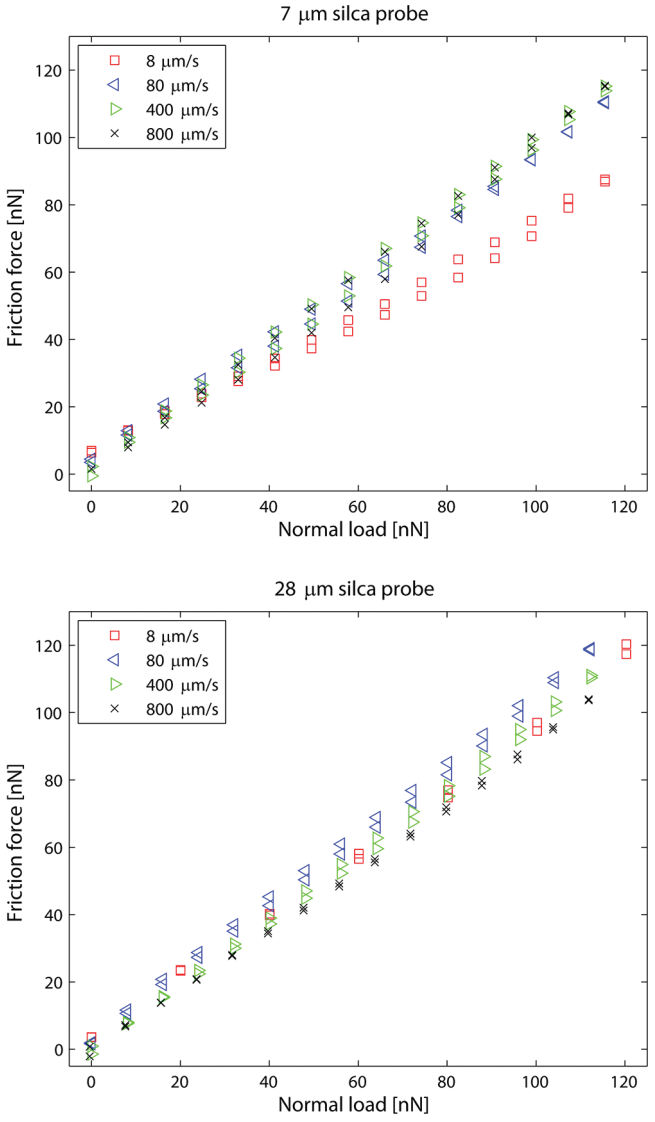

Figure 3. Friction vs normal load between a 7 μm silica probe and a microstructured silicon surface (top) and a 28 μm silica probe and a microstructured silicon surface obtained at four different sliding velocities, in the range 8−800 μm/s.

present case. One explanation for the change in probe−needle interaction could be that possible capillary effects become more significant at low velocities. However, it is difficult to imagine why this should be the case only for the smaller probe and only at high applied load. We therefore suggest that a change in the needle relaxation mechanism is needed to explain the observed decrease in friction. One scenario could be that the smaller probe is sliding between two arrays of needles. These needles will thus bend with a restoring force opposite to the probe motion which will be released when the probe has past. Alternatively, the needles can slide around the probe, which at high applied load will lead to a smaller bending angle of the needles and thus lower the friction. On the basis of the results, we suggest that such an alternative slower relaxation process exists and becomes significant at low sliding velocity and high applied load. Although this is a result of a special case related to this particular system, it possibly illustrates how the friction force deviates from Amontons' law when the nature of the energy dissipating mechanism changes with the applied load and sliding velocity. A similar observation has previously been seen in the case of friction between polyelectrolyte coated surfaces in aqueous solution where the normal load was found to be carried by an electrostatic double layer force at low applied loads and by steric repulsion between the polyelectrolyte chains at higher applied loads.[23] In this case, the friction behavior changed dramatically when the main load carrying force, and thereby the energy dissipating mechanism, was changed. Probably, this is also the reason why Amontons' law has been shown to fail for some system when investigated over an extended range of applied loads since the main energy dissipating mechanism for most systems are likely to change over an extended range of applied loads.

In the case of shearing, a d = 28 μm silica probe against the microstructured surface (Figure 3B) the average friction force is found to be independent of sliding velocity and a linear relationship between friction and applied load is again observed. When the probe is significantly larger than the dimensions of the surface structures the second relaxation mechanism where the needles slide around the probe becomes unavailable, and it is thus in agreement with the above suggested mechanism that the friction in this case does not change at low sliding velocities. Interestingly, it is also observed that the measured friction coefficient (μ = 0.96 ± 0.04), within experimental error, is identical to the friction coefficient (μ = 0.93 ± 0.04) found when using the smaller probe. This suggests that the average friction force is independent of the number of macroscopic contact points. It is often suggested that Amontons' law, which states that friction is independent of the macroscopic contact area and dependent only on the applied load, holds because the actual contact area of rough surfaces changes with applied load in such a way that the friction depends on the actual surface area but not on the apparent contact area. However, in the present case, it is difficult to make the same connection, because the number of microneedles in contact with the probe scales with the probe size. Instead we suggest that this is a direct consequence of the linear relationship between the friction and applied load, as will be discussed further in relation with Figure 4A. If a given applied load of the smaller probe leads to a certain degree of bending of a few microneedles, the same applied load of the larger probe will lead to less bending of a larger number of microneedles. However, because of the linearity of the response, the friction experienced by bending many microneedles to a smaller extent adds up to the same friction experienced by bending few microneedles to a larger extent. This can in the simplest form be expressed as

$$F_{\text{fric}} = \sum_{k=1}^{n} \mu_k \frac{F_N}{n} = \mu_k F_N \qquad (4)$$

where F_N is the normal applied load, n is the number of bent needles, and μ_k is a constant given the proportionality between the applied normal load and the bending contribution to the friction force from the kth needle.

Comparison with Some Microscopic Models. The observed linearity between the friction force and applied load in our experiments can be rationalized by considering Figure 4A. The interaction between the probe and a given microneedle leads to bending of the needle which gives rise to a restoring force $F_\perp$, which has to be balanced by an external force if the system is in equilibrium. This restoring force has a component normal to the surface (but not normal to the bent needle) which is balanced by the applied normal load, F_N, and a lateral component which is balanced by a torsional cantilever deflection which we recognize as the friction force, F_{fric}. These two components always have a linear relationship, $F_{\text{fric}} = F_N \tan \alpha$. It should be noted that the lateral force is not equivalent to the local intrinsic friction force which acts in the plane of the surface contact and not to the substrate and that the angle, α, as well as the local restoring force, will change with the applied load and the relative position of the probe and the needle. However, as we define the friction force as the space and time average of

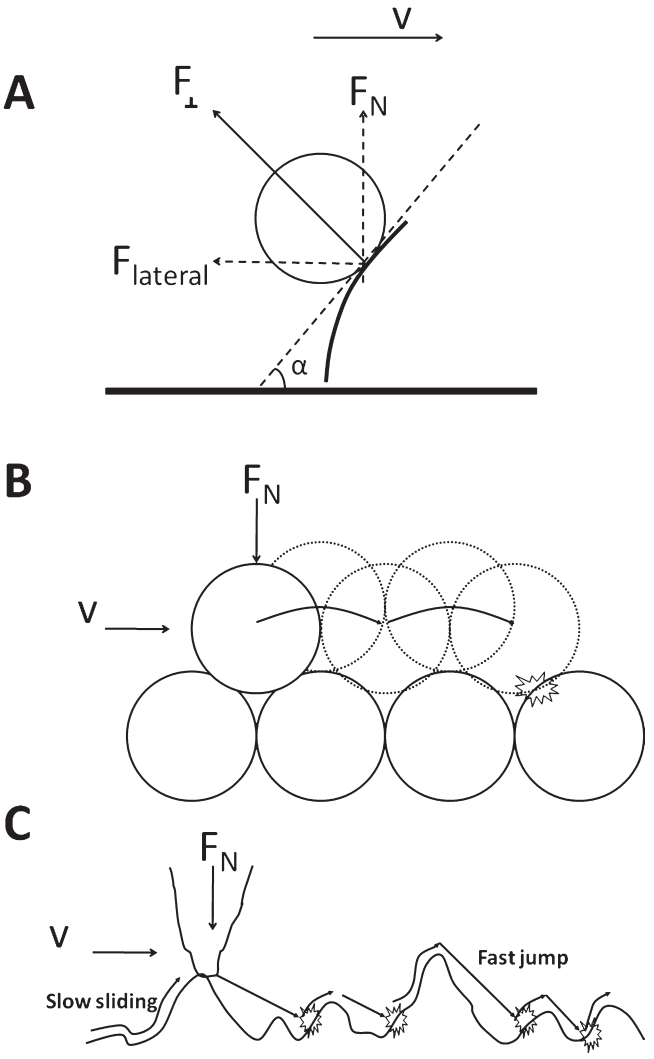

Figure 4. Schematic illustrations of three microscopic friction models. (A) The coupling between the normal and the lateral force component of the elastic restoring force of a bent needle can be used to explain the linear relationship between friction force and applied load observed in our experiments. (B) The Cobblestone model suggests a mechanism for atomic friction. (C) The stick-and-slip model suggests a mechanism for friction between rough surfaces.

lateral force measured while moving the probe parallel to the sample substrate under an average applied force these variations are invisible in Figure 3. The friction can thus also be thought of as the bending energy that is lost when the needle is released and returns to its rest position although this view probably is too simple since the needle is not end-loaded during the entire bending event. A more likely situation is that the needle in the beginning is loaded at a position away from the apex of the needle, and as it starts to bend the probe simultaneously slides toward the apex of the needle, whereafter the needle finally is released. This means that on top of the lost bending energy comes the energy lost due to the intrinsic friction between the probe and the needle when the probe slides along the bent needle. The question of the effect of intrinsic friction for interaction between inelastic and undeformable surface asperities with known slopes has been modeled and measured by Makinson[38] more than 60 years ago, and more lately also demonstrated by Ruan and Bhushan.[5] To understand the special abilities of geckos to climb walls and ceilings several studies have been focused on how directional arrays of microscopic setae can lead to shear stress induced adhesion.[39−41] Related to this, studies of friction between model surfaces consisting of relatively closed-packed micrometer sized polymer fibers have also showed significantly higher friction than corresponding nonstructured surfaces of the same material.[42−44] Studies of this kind of systems have also revealed that for fibers with a tilt angle, the friction is higher when sliding with the fiber orientation than when sliding against the fiber orientation. This somehow counterintuitive result is suggested to be a consequence of the larger penetration depth of the sliding probe when sliding with the fiber orientation due to the lower bending elasticity in this sliding geometry.[44] This also suggests that both the lost bending energy and the increased surface contact are responsible for the increase in friction. However, no models have to our knowledge fully accounted for the coupling between lateral elastic deformation and intrinsic friction as observed in this study.

Several models and simulation results[22,24,25] suggest that the validity of Amontons' law is due to a linear coupling between the applied load and the real contact area. Due to the finite number of contact points determined by the density of needles, their elastic response and the applied load, this is not an obvious explanation for the validity of Amontons' law in this case. However, another purely mechanical model introduced by Israelachvili seems to be able to explain the intrinsic interatomic friction without including any information about neither the apparent nor the real surface area. In this model, which is known as the Cobblestone model,[45,46] the friction force is related to the work done against the applied load when a surface atom on the upper surface has to "climb" over a surface atom on the lower surface (see Figure 4B). In this model, the energy is dissipated because the upper atom after climbing the lower atom collides with a neighboring atom on the lower surface; an event where the potential energy is transformed to random vibrational energy (heat). The reason why this model is independent of the number of contact points for nonadhering surfaces is that if more contact points exist, then the load carried by each contact point decreases to a fraction given by the total applied load divided by the number of contact points similar to the discussion in relation to eq 4. The Cobblestone model is closely related to a more macroscopic model termed the stick-and-slip model (although the climb-and-jump model would be a more appropriate name) by Rabinowicz[47] where the friction force is related to the work needed for a surface asperity on the upper surface to climb a surface asperity on the lower surface against the applied load (see Figure 4C). We find significant similarities between the cobblestone and stick-and-slip models and our situation where work is needed to bend a microneedle is given by the applied load (this can be compared to climbing a surface asperity against the applied load) and the energy is dissipated when the needle is released (this can be compared to the energy that is dissipated when the upper surface slips and collides with a neighboring surface asperity on the lower surface). The main difference between the two situations is that in our system, the surface features are not only climbed but also laterally elastically deformed. We suggest that for many systems a combination of the two situations will be found, which thus calls for a more advanced model.

3. CONCLUSION

In this study, Amontons' law was challenged by friction measurements between a spherical silica particle and a microstructured silicon surface consisting of arrays of vertical microneedles. Amontons' law was challenged in terms of linearity between friction force and applied load, a change in size of the spherical silica particle and variation in the sliding velocity. First, by looking at the friction force as a function of time and space, the friction force was observed to oscillate with a period related to the spacing between the microneedles when using a small silica particle, while showing a noisy random variation when using a larger silica particle. Because the friction in both cases is expected

to be related to bending and releasing individual needles, this shows how the direct evidence of the energy dissipating mechanism becomes hidden when the size of the sliding body becomes much larger than the surface features. Looking at the average friction force as a function of applied load, our results show that Amontons' law is valid for this system since a linear relationship between friction and applied load was achieved and the friction force was found to be independent of the size of the silica particle and the sliding velocity. One exception from this was observed when using the smallest silica particle and the lowest sliding velocity. We suggest that the deviation from Amontons' law in this particular case is a consequence of a change in the bending-relaxation mode of the microneedles which only is possible at low sliding velocities and when the particle size approaches the dimensions of the spacing between the microneedles. However, although this explanation apply to a specific situation for this particular system the observation illustrates a much more fundamental principle. The result illustrates that Amontons' law is fulfilled only as long as the main energy dissipating mechanism is not changing with the applied load and sliding velocity.

Because Amontons' law is a purely phenomenological and macroscopic law, our system and results were also evaluated against some existing microscopic models. It was concluded that models where Amontons' law is validated by a presumably linear increase in contact area or in the number of contact points with the applied load is not an obvious explanation for the Amontonian behavior in the present case. Instead, we found strong similarities between our system and a set of mechanical models, with the Cobblestone model being the most well-known, where energy is dissipated when the upper surface has to climb a surface asperity on the lower surface against the applied load and subsequently slips and collides with a neighboring surface asperity. In our system, the results suggest that the energy to a large extent is dissipated due to a process where the microneedles are first bending (elastically deformed) then subsequently released so that they can returned to their rest position. We suggest that for many systems, both climbing and elastic deformation has to be taken into account.

AUTHOR INFORMATION

Corresponding Author

*To whom correspondence should be addressed. Email: esben@kth.se, fax: +46 8208998.

ACKNOWLEDGMENT

This work was financed by the Swedish Foundation for Strategic Research (SSF) through the programs "Multi-Functional Pore arrays in Silicon" and "Microstructure, Corrosion and Friction Control".

REFERENCES

(1) Ludeman, K. C. In *Modern Tribology Hanbook*; Bhushan, B., Ed.; CRC Press; Boca Raton, FL, 2001; Vol. 1, pp 205−230.

(2) Gnecco, E.; Bennewitz, R.; Pfeiffer, O.; Socoliuc, A.; Meyer, E. In *Nanotribology and Nanomechanics*, 2nd ed.; Bhushan, B., Ed.; Springer: Berlin, 2008; pp 557−600.

(3) Berman, A.; Drummond, C.; Israelachvili, J. *Tribol. Lett.* **1998**, *4*, 95–101.

(4) Gao, J.; Luedtke, W. D.; Gourdon, D.; Ruths, M.; Israelachvili, J. N.; Landman, U. *J. Phys. Chem. B* **2004**, *108*, 3410–3425.

(5) Ruan, J.-A.; Bhushan, B. *J. Appl. Phys.* **1994**, *76*, 5022–5034.

(6) Kusy, R. P.; Whitley, J. Q. *J. Biomech.* **1990**, *23*, 913–925.

(7) Koinkar, V. N.; Bhushan, B. *J. Appl. Phys.* **1997**, *81*, 2472–2479.

(8) Persson, B. N. J.; Albohr, O.; Tartaglino, U.; Volokitin, A. I.; Tosatti, E. *J. Phys.: Condens. Matter* **2005**, *17*, R1–R62.

(9) Stiernstedt, J.; Nordgren, N.; Wagberg, L.; Brumer, H.; Gray, D. G.; Rutland, M. W. *J. Colloid Interface Sci.* **2006**, *303*, 117–123.

(10) Lancaster, J. K. *Tribol. Int.* **1990**, *23*, 371–389.

(11) Yoshizawa, H; Chen, Y. L.; Israelachvili, J. *J. Phys. Chem.* **1993**, *97*, 4128–4140.

(12) Vigil, G.; Xu, Z.; Steinberg, S.; Israelachvili, J. *J. Colloid Interface Sci.* **1994**, *165*, 367–385.

(13) Binggeli, M; Mate, C. M. *Appl. Phys. Lett.* **1994**, *65*, 415–417.

(14) Ruths, M.; Ohtani, H; Greenfield, M. L.; Granick, S. *Tribol. Lett.* **1999**, *6*, 207–214.

(15) Limpoco, F. T.; Advincula, R. C.; Perry, S. S. *Langmuir* **2007**, *23*, 12196–12201.

(16) Feiler, A. A.; Bergstrom, L.; Rutland, M. W. *Langmuir* **2008**, *24*, 2274–2276.

(17) Bhushan, B.; Israelachvili, J. N.; Landman, U. *Nature* **1995**, *374*, 607–616.

(18) Raviv, U.; Giasson, S.; Kampf, N.; Gohy, J. F.; Jerome, R.; Klein, J. *Nature* **2003**, *6954*, 163–165.

(19) Persson, B. N. J. *Phys. Rev. B* **1993**, *48*, 18140–18158.

(20) Dedinaite, A.; Pettersson, T.; Mohanty, B.; Claesson, P. M. *Soft Matter* **2010**, *6*, 1520–1526.

(21) Pilkington, G. A.; Thormann, E.; Claesson, P. M.; Fuge, G. M.; Fox, O. J. L.; Ashfold, M. N. R.; Leese, H.; Mattia, D.; Briscoe, W. H. *Phys. Chem. Chem. Phys.* **2011**, *13*, 9318–9326.

(22) Bowden, F. P.; Tabor, D. *The Friction and Lubrication of Solids*; Clarendon Press: Oxford, U.K., 1950.

(23) Dedinaite, A.; Thormann, E.; Olanya, G.; Claesson, P. M.; Nyström, B.; Kjøniksen, A.-L.; Zhu, K. *Soft Matter* **2010**, *6*, 2489–2498.

(24) Greenwood, J. A.; Williamson, J. B. P. *Proc. R. Soc. London, Ser. A* **1966**, *295*, 300–319.

(25) Mo, Y.; Turner, K. T.; Szlufarska, I. *Nature* **2009**, *457*, 1116–1119.

(26) Mo, Y.; Szlufarska, I. *Phys. Rev. B* **2010**, *81*, 035405.

(27) Chang, C.; Wang, Y. F.; Kanamori, Y.; Shih, J. J.; Kawai, Y.; Lee, C. K.; Wu, K. C.; Esashi, M. *J. Micromech. Microeng.* **2005**, *15*, 580–585.

(28) Sader, J. E.; Chon, J. W. M.; Mulvaney, P. *Rev. Sci. Instrum.* **1999**, *70*, 3967–3969.

(29) Thormann, E.; Pettersson, T.; Claesson, P. M. *Rev. Sci. Instrum.* **2009**, *80*, 093701.

(30) Pettersson, T.; Nordgren, N.; Rutland, M. W.; Feiler, A. *Rev. Sci. Instrum.* **2007**, *78*, 093702.

(31) Zhao, N.; Xu, J.; Xie, Q. D.; Weng, L. H.; Guo, X. L.; Zhang, X. L.; Shi, L. H. *Macromol. Rapid Commun.* **2005**, *26*, 1075–1080.

(32) Gao, H. J.; Wang, X.; Yao, H. M.; Gorb, S.; Arzt, E. *Mech. Mater.* **2005**, *37*, 275–285.

(33) Bhushan, B.; Koch, K.; Jung, Y. C. *Appl. Phys. Lett.* **2008**, *93*, 093101.

(34) Lai, Y. H.; Lin, C. Y.; Chen, H. W.; Chen, J. G.; Kung, C. W.; Vittal, R.; Ho, K. C. *J Mater. Chem.* **2010**, *20*, 9379–9385.

(35) Thormann, E.; Simonsen, A. C.; Hansen, P. L.; Mouritsen, O. G. *Langmuir* **2008**, *24*, 7278–7284.

(36) Adhesion due to capillary condensation was observed between flat silica, and the friction thus does not strictly follow Amontons law in this case.

(37) Where F is the maximum lateral (friction) force, l is the rod/needle length, E is Youngs modulus of silicon, I is the moment of inertia of the rod/needle, d is the diameter of the silica probe, and k_t is the torsional spring constant of the cantilever.

(38) Makinson, K. R. *Trans. Faraday Soc.* **1948**, *44*, 279–282.

(39) Urbakh, M.; Klafter, J.; Gourdon, D.; Israelachvili, J. *Nature* **2004**, *430*, 525–528.

(40) Autumn, K.; Dittmore, A.; Santos, D.; Spenko, M.; Cutkosky, M. *J. Exp. Biol.* **2006**, *209*, 3569–3579.

(41) Tian, Y.; Pesika, N.; Zeng, H. B.; Rosenberg, K.; Zhao, B. X.; McGuiggan, P.; Autumn, K.; Israelachvili, J. *Proc. Natl. Acad. Sci. U.S.A.* **2006**, *103*, 19320–19325.

(42) Lee, J.; Majidi, C.; Schubert, B.; Fearing, R. S. *J. R. Soc. Interfaces* **2008**, *5*, 835–844.
(43) Schubert, B.; Lee, J.; Majidi, C.; Fearing, R. S. *J. R. Soc. Interfaces* **2008**, *5*, 845–853.
(44) So, E.; Demirel, M. C.; Wahl, K. J. *J. Phys. D: Appl. Phys.* **2010**, *43*, 045403.
(45) Ruths, M.; Israelachvili, J. N. In *Nanotribology and Nanomechanics*, 2rd ed.; Bhushan, B., Ed.; Springer: Berlin, 2008; pp 417−497.
(46) Berman, A. D. In *Modern Tribology Hanbook*; Bhushan, B., Ed.; CRC Press: Boca Raton, FL, 2001; Vol. 1, pp 568−600.
(47) Rabinowicz, E. *Friction and Wear of Material*, 2nd ed.; Wiley: New York, 1995.